

Monte Carlo simulation of subsurface ordering kinetics in an fcc–alloy model

M. Kessler, W. Dieterich

Fachbereich Physik, Universität Konstanz, D-78457 Konstanz, Germany

and A. Majhofer

Institute of Experimental Physics, Warsaw University, ul. Hoża 69,

PL-00681 Warszawa, Poland

(March 1, 2001)

Within the atom–vacancy exchange mechanism in a nearest–neighbor interaction model we investigate the kinetics of surface–induced ordering processes close to the (001) surface of an fcc A_3B –alloy. After a sudden quench into the ordered phase with a final temperature above the ordering spinodal, $T_f > T_{sp}$, the early time kinetics is dominated by a segregation front which propagates into the bulk with nearly constant velocity. Below the spinodal, $T_f < T_{sp}$, motion of the segregation wave reflects a coarsening process which appears to be slower than predicted by the Lifschitz–Allen–Cahn law. In addition, in the front–penetrated region lateral growth differs distinctly from perpendicular growth, as a result of the special structure of antiphase boundaries near the surface. Our results are compared with recent experiments on the subsurface ordering kinetics at Cu₃Au (001).

05.70.Ln,61.30.Hn,64.60.-i

1. INTRODUCTION

Near a surface, kinetic processes connected with first–order phase transitions are generally modified in a fundamental manner relative to the corresponding bulk process. Well–known examples are surface–induced spinodal decomposition and nucleation phenomena,^{1–6} whose understanding and control is of major concern in modern thin film and nanostructure technologies. Surface kinetic effects during ordering transitions in metallic binary alloys^{7,8} acquire special interest from the scientific point of view as their (low–temperature) ordered phase normally is characterized by a multicomponent order parameter, whose components in general couple differently to a crystal surface with a particular symmetry and hence will display different relaxational behaviors. In such cases, the surface is expected to induce rich dynamical behavior of the order parameter, predominantly at short times.

A well–studied system is the (001) surface of Cu₃Au, an fcc–alloy which undergoes a first–order bulk transition from the disordered phase to the ordered $L1_2$ structure at a temperature $T_0 = 663K$. In the bulk, Au–atoms preferentially occupy one of the four simple–cubic sublattices of the underlying fcc–lattice. The ground state therefore is 4–fold degenerate, and there exist two types of antiphase boundaries separating the 4 types of energetically equivalent equilibrium domains. Several peculiar modifications of order near the (001) surface of Cu₃Au have been reported. Below the ordering temperature T_0 the (001)–surface displays disorder–wetting.^{9–11} Moreover, above T_0 , the tendency of Au–atoms to enrich in the outermost (first) layer leads to an oscillatory segregation profile with successive Au–depletion and enrichment in even and odd layers, respectively.^{12–15} This

profile decays towards the bulk on a length scale given by the bulk–correlation length $\xi(T)$, which on extrapolation to lower temperatures appears to diverge at the spinodal temperature $T_{sp} \simeq T_0 - 30K$.^{16,12,17} Intriguing non–equilibrium behavior of segregation amplitudes has been detected recently by time–resolved X –ray experiments.¹⁸ After a quench from an initial temperature $T_i > T_0$ to a final temperature $T_f < T_0$ the initial surface segregation profile induces a segregation front which rapidly progresses towards the bulk, while lateral order was found to develop on longer time–scales. This two–stage ordering process was interpreted recently in terms of time–dependent Ginzburg–Landau (GL) theory.¹⁹ Although restricted to one dimension and to the limit of vanishing thermal noise, this theory successfully yields the difference in time–scales for perpendicular and lateral ordering and identifies an anisotropy of the evolving domain structure within a characteristic penetration depth of the segregation front.

Motivated by these studies of the subsurface ordering kinetics of Cu₃Au (001), our aim here is to gain more insight into possible surface–induced ordering scenarios in A_3B fcc–alloys with the help of dynamical Monte Carlo simulations. As a minimal model with respect to equilibrium properties we choose a lattice with nearest–neighbor interactions among A and B –atoms, known to account reasonably for the bulk phase diagram of the Cu – Au system. Our dynamic algorithm relies on the vacancy mechanism, where elementary atomic moves consist in an exchange of (A)Cu– or (B)Au–atoms with vacancies V .^{20–24} This kind of ABV –model, which has been used before by Frontera et al. in an investigation of the bulk ordering kinetics in A_3B alloys,²⁵ is physically more realistic than the conventional direct AB –exchange kinetics and will simultaneously allow us to scale the simulated

surface-induced growth rates with the self-diffusion coefficient of A - and B -atoms.

The main results of our simulations are: (i) the occurrence of two distinctly different modes of progression of the segregation front, depending on the final temperature T_f to lie significantly above the spinodal temperature, $T_f > T_{sp}$ (quench into the metastable regime) or below, $T_f < T_{sp}$ (quench into the unstable regime), (ii) an early-time linear (constant velocity) growth behavior of the segregation front in the case $T_{sp} < T_f < T_0$ and a characteristic time t^* , where this linear growth decelerates. Below T_{sp} it changes over to a growth roughly proportional to $t^{1/4}$ up to our longest computing times. (iii) A different behavior of lateral growth in the near-surface region. In connection with this we give a detailed description of the persistent anisotropy in the near-surface domain-structure.

The paper is organized as follows. Section 2 defines our model; its bulk properties and equilibrium surface properties are tested in Section 3. The subsequent Section 4 discusses in detail the processes of perpendicular and lateral ordering. Our findings have strong relevance to the temperature quench experiments on Cu_3Au described above, although the present model based on spatially uniform parameters for nearest-neighbor interactions cannot be expected to work quantitatively. In fact it implies an enhancement of static lateral order near the surface as compared to the bulk, an effect not borne out in the real material Cu_3Au . Enhanced lateral order at the (001)-surface, however, seems to be observable in the fcc-alloy Cu_3Pd .²⁶ Concluding remarks are presented in Section 5.

2. MODEL AND SIMULATION METHOD

Consider a lattice of $N \times N \times M$ fcc-cells with periodic boundary conditions in the x - and y -direction. Along the z -axis our system is bound between two free surfaces. Atomic layers normal to the z -direction with distance a are labeled by n with $1 \leq n \leq 2M + 1$. Each lattice site i can be occupied either by an A -atom, or a B -atom, or a vacancy so that the corresponding occupation numbers c_i^A , c_i^B and c_i^V satisfy $c_i^A + c_i^B + c_i^V = 1$. In our simplified alloy model only pairwise nearest-neighbor interactions are taken into account. The configurational Hamiltonian then reads

$$H = \sum_{\langle i,j \rangle} [V_{AA}c_i^A c_j^A + V_{BB}c_i^B c_j^B + V_{AB} (c_i^A c_j^B + c_i^B c_j^A)], \quad (1)$$

where the summation is over nearest-neighbor pairs.²⁷ In all our investigations we assume a very small amount of vacancies such that macroscopic equilibrium properties remain essentially unaffected by the vacancies. Hence, for equilibrium considerations, we can ignore the vacancies and introduce spin variables $s_i = 2c_i^A - 1 = \pm 1$ by

which equation (1) is mapped onto the spin-1/2 Ising model,

$$H_I = -J \sum_{\langle i,j \rangle} s_i s_j - h \sum_i s_i - h_1 \sum_i s'_i \quad (2)$$

with

$$J = -\frac{1}{4} (V_{AA} + V_{BB} - 2V_{AB}) \quad (3)$$

$$h = 3(V_{BB} - V_{AA}) \quad (4)$$

The surface field

$$h_1 = V_{AA} - V_{BB} \quad (5)$$

acts only on spins in the surface layers $n = 1$ and $n = 2M + 1$. Bulk properties at fixed composition only depend on the parameter J . Regarding the $\text{Cu}(A)$ - $\text{Au}(B)$ system, it is natural to assume $V_{BB} > 0$ because of the larger size of Au -atoms relative to the Cu -atoms, whereas $V_{AA} < 0$, $V_{AB} < 0$ such that bulk interactions will favor “anti-ferromagnetic” ordering $J < 0$. Near the stoichiometric composition A_3B the emerging bulk $L1_2$ -structure is described by a 4-component order parameter, one conserved concentration variable ψ_0 and three non-conserved components ψ_1, ψ_2 , and ψ_3 . These are defined via the differences $m_\alpha = \langle c_i^A \rangle - \langle c_i^B \rangle$; $i \in \alpha$; of averaged A - and B -occupations of the four equivalent simple-cubic sublattices $\alpha = 1, \dots, 4$ building the fcc lattice, namely⁸

$$\psi_0 = m_1 + m_2 + m_3 + m_4$$

$$\psi_1 = m_1 - m_2 - m_3 + m_4$$

$$\psi_2 = m_1 - m_2 + m_3 - m_4$$

$$\psi_3 = m_1 + m_2 - m_3 - m_4$$

Each non-conserved component describes a layerwise modulation of the B -atom concentration along one of the three cubic axes. The ground state shows 4-fold degeneracy, where the four types of equivalent ordered domains have components $(\psi_1, \psi_2, \psi_3)/\bar{\psi} = (-1, 1, 1); (1, -1, 1); (1, 1, -1)$ and $(-1, -1, -1)$. In the ground state ($T = 0$) the amplitude ψ takes the value $\bar{\psi} = 2$. Local order parameters to be used in our subsequent simulations are defined in terms of averages over one fcc-cell. Order parameter profiles and structure factors are obtained by averaging over 10 independent simulation runs.

With the above choice of interaction parameters we obtain a negative surface field $h_1 < 0$, favoring an enrichment of B -atoms in the outermost layers $n = 1$ and

$n = 2M + 1$. This is to be expected in view of the BB -repulsion. As shown by Schweika and Landau²⁸ on the basis of the Hamiltonian, (2), the value $h_1/|J| = -4$ is consistent with the experimentally measured concentration of Au-atoms of about 50% in the surface layer of $\text{Cu}_3\text{Au}(001)$ near the ordering temperature T_0 .¹²

As explained in the Introduction, our kinetic model will be based on the atom–vacancy exchange mechanism and hence will involve all three interaction parameters appearing in (1). In order to deal with only one energetic parameter in the Hamiltonian, we choose $V_{BB} = -V_{AA} = -V_{AB} > 0$; $|J| = V_{BB}/2$, which is consistent with $h_1 = -4|J|$.

To affect an elementary atomic move we randomly select a nearest-neighbor vacancy–atom pair and calculate the vacancy–atom exchange probability by using the Metropolis algorithm. Throughout all of our calculations the mean vacancy density is taken as $c^V \simeq 6.1 \cdot 10^{-5}$, which amounts to 128 vacancies in a system of typical size $N = 64$; $M = 128$ with $4N^2M$ sites. One Monte Carlo step (MCS) consists of $4N^2M$ attempted moves and is independent of c^V . Clearly, in an actual material the vacancy concentration generally will depend on temperature and the amount of A - and B -atoms. Our kinetic model with fixed c^V therefore does not allow us to compare time-scales of vacancy-mediated processes taking place at different temperatures and composition. However, our subsequent analysis of the ordering kinetics focuses on the exact stoichiometric composition A_3B ($c^B = 0.25$) and a narrow temperature range near T_0 where changes of c^V are expected to be of minor importance.

3. BULK PROPERTIES AND SURFACE SEGREGATION

In this section we discuss some elementary properties of our model, part of which are already known in the literature but they are needed here as a test of our kinetic algorithm and as a basis for the subsequent investigations of surface-induced kinetic properties. Fig. 1a shows the phase diagram in the vicinity of $c^B \simeq 0.25$ as obtained from simulations of a system with size $M = N = 64$ and periodic boundary conditions in all directions. To obtain the lines of coexistence between the disordered phase and the ordered $L1_2$ -structure it was sufficient for the present purpose to analyze the decay of a perfectly ordered initial state upon thermalization at different temperatures. In particular, we obtain for the ordering temperature $k_B T_0 \simeq 1.83|J|$, in good agreement with literature data ($k_B T_0 \simeq 1.85|J|$).^{28,29} Fig. 1a reasonably reproduces the bulk phase diagram of the Cu–Au system near $c^B = 0.25$. Furthermore we remark that the present model displays a surface transition at a critical temperature $T_{cs} > T_0$, which we estimate as $T_{cs} \simeq 1.12 T_0$ for $c^B = 0.25$. Below T_{cs} the outermost

layers with nearly equal amounts of A - and B -atoms develop a lateral (1,1)-superstructure. With respect to Cu_3Au , the existence of a surface critical temperature clearly is an artefact of the present model, connected with the fact that fcc lattice models based on spatially uniform short range interactions are unable to account for surface-induced disordering.²⁸ The (001)-surface of the $L1_2$ -structure of Cu_3Pd , on the other hand, appears to favor lateral ordering.²⁶

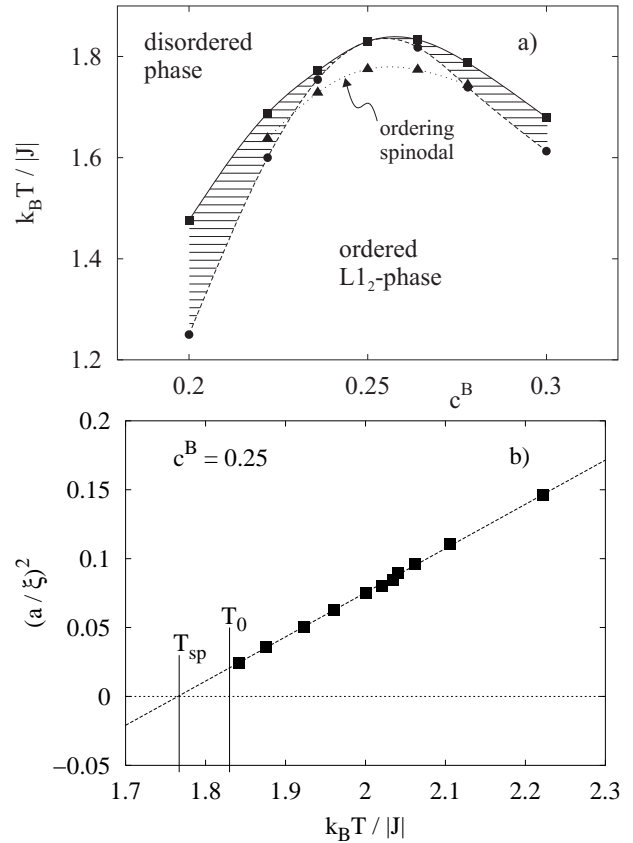


FIG. 1. (a) Phase diagram of the AB -binary alloy model in the vicinity of $c^B = 0.25$. Data points from simulations are connected by smooth lines. Full line (■) and dashed line (●): boundaries of the disordered phase and the ordered $L1_2$ -structure, with the two-phase coexistence region in between. Dotted line (▲): ordering spinodal. (b) Plot of $(a/\xi)^2$ versus temperature at $c^B = 0.25$, illustrating the determination of the spinodal temperature.

Next we estimate the spinodal temperature in a manner as done experimentally.¹² In the disordered phase B -atoms are known to show an oscillatory segregation profile near the (001) surface, with enrichment and depletion in odd and even layers, respectively. When atoms in the outermost layers are identified with sublattices $\alpha = 3$ and 4, the segregation amplitude is given by the order parameter component ψ_3 . At the surface, its magnitude is determined by the surface field h_1 . Below the surface it decays towards the bulk on a length scale given by the bulk correlation length $\xi(T)$.¹³ Extrapolation of data for $\xi(T)$

to lower temperatures according to $\xi(T) \sim (T - T_{sp})^{-1/2}$ allows one to estimate the spinodal temperature T_{sp} . Experimentally, $T_0 \simeq 663\text{ K}$ and $T_{sp} \simeq T_0 - 30\text{ K}$ near the stoichiometric composition of Cu_3Au .¹² Application of this procedure to our simulation data is illustrated in Fig. 1b and yields the ordering spinodal displayed in Fig. 1a. At $c^B = 0.25$ we find $T_{sp}/T_0 \simeq 0.967 \pm 0.003$.³⁰ This is somewhat larger than the experimental value but reasonably close in view of the simplicity of our model. Simultaneously we get (see Fig. 1b) $\xi(T_0) \simeq 6a$, which again agrees fairly well with experiment.¹² For metallic alloys where short range interactions prevail, it is well known that the spinodal and the nucleation regime connect smoothly.³ The qualitative significance of the spinodal temperature, however, becomes apparent from Fig. 2a and b. There we compare bulk patterns of the order parameter component ψ_1 at a time $t = 7 \cdot 10^3$ MCS after a sudden quench from a purely random initial state to final temperatures $T_f \simeq 0.972 T_0 > T_{sp}$ (Fig. 2a) and $T_f = 0.963 T_0 \lesssim T_{sp}$ (Fig. 2b), respectively. Snapshots were taken in a section parallel to the (xy) -plane.

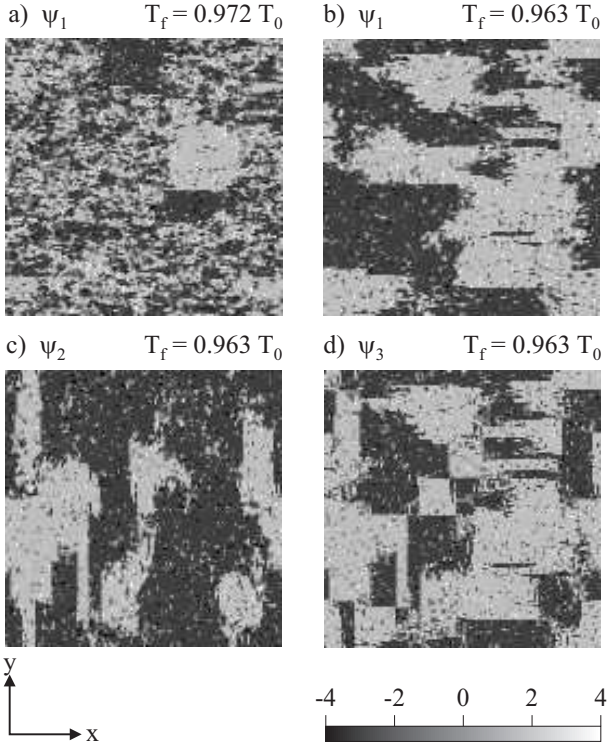


FIG. 2. Bulk domain patterns ($c^B = 0.25$) at a time $t = 7 \cdot 10^3$ MCS after a quench from random initial conditions. Grey scales reflect values of the local order parameters between extremal values 4 and -4 .

(a) ψ_1 -pattern at a final temperature $T_f = 0.972 T_0 > T_{sp}$. (b)-(d) patterns of ψ_1, ψ_2, ψ_3 at $T_f = 0.963$, making evident the two types of domain walls and the anisotropy of the evolving structures.

In the first case only small ordered domains have nucleated in an essentially disordered background (Fig. 2a).

By contrast in Fig. 2b we observe a continuous domain pattern typical of spinodal ordering. At that temperature ($T_f = 0.963 T_0$) the same type of patterns is seen also at shorter observation times. For a complete characterization of the evolving domains in Fig. 2b we need in addition the ψ_2 - and ψ_3 -patterns displayed in Figs. 2c and 2d. From the grey-scales in Figs. 2b-2d one can easily see that inside a domain we have $\psi_1 \psi_2 \psi_3 < 0$. Furthermore, the well-known two types of antiphase boundaries³¹ are recovered. For example, boundaries where ψ_1 and ψ_3 simultaneously change sign in the y -direction are the “low-energy” (type-1) domain walls and in fact cost no energy in our nearest-neighbor model. These walls are almost completely flat and turn out to be rather stable. On the other hand, boundaries where ψ_1 and ψ_3 simultaneously change sign in the x -direction are “high-energy” (type-2) walls where curvature-driven coarsening is much more effective than for type-1 walls. Bulk coarsening effects at quench temperatures lower than those considered here have been simulated in detail by Frontera et al.²⁵ These authors obtained coarsening exponents n smaller than that in the conventional Lifschitz–Allen–Cahn coarsening law, where $n = 1/2$, and interpreted their findings in terms of the presence of those stable low-energy walls.

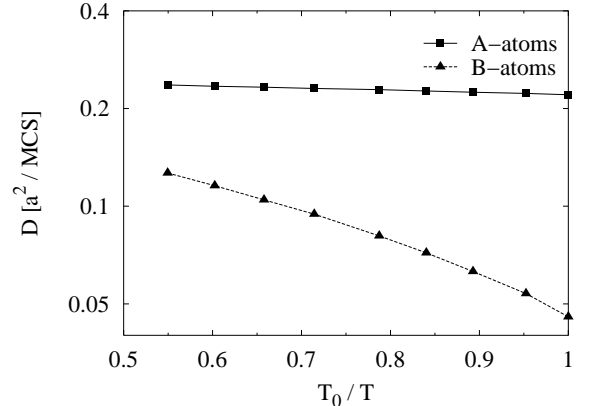


FIG. 3. Temperature-dependent diffusion constants of A - and B -atoms in an Arrhenius representation.

In addition we extract tracer diffusion coefficients from our model, restricting ourselves again to $c^B = 0.25$ and to temperatures above but close to T_0 . Diffusion coefficients D_A and D_B for A - and B -atoms are obtained in the usual way from time-dependent mean-square displacements and are plotted in Fig. 3 in an Arrhenius representation. Since in our model $V_{AA} = V_{AB}$, the energy remains essentially unchanged by a jump of an A -atom so that D_A is found to be nearly temperature-independent. On the other hand, because of the B - B -repulsion the B -atoms will migrate more slowly than the A -atoms, and D_B decreases upon cooling. As indicated already, in a real system c^V will grow with temperature. Therefore the individual experimental curves $\log D_A$ or $\log D_B$ ver-

sus $1/T$ will be steeper than those in Fig. 3. However, the ratio D_A/D_B roughly agrees with experimental data for Cu_3Au , where $D_A/D_B \simeq 1.45$ at $T/T_0 \simeq 1.7$,³² while we find $D_A/D_B \simeq 2$ at the same T/T_0 -ratio.

Let us close this section by a brief remark on the distribution of vacancies in our system with free surfaces. First of all, vacancies tend to enrich in the outermost layers. For example at $T/T_0 = 0.972$ we find a surface vacancy concentration of about $c_{\text{surface}}^V \simeq 2.5 \cdot 10^{-3}$, much larger than the overall concentration. The fact that vacancies are expelled from the bulk suggests that in fact we are dealing with a model for a stable solid which, when regarding the complete ternary (ABV)-system, would be phase-separated from the “vacuum” (vacancy-rich) phase. Furthermore, when analyzing the above-mentioned layered structure along the z -axis caused by surface segregation, we find that vacancies deplete in the AB -layers and enrich in the A -layers. The reason is that the BB repulsive energy in AB -layers becomes minimized when vacancies avoid B -sites. The resulting oscillations in the vacancy-density along the z -axis have an amplitude of about 30 percent relative to the average vacancy density.

4. SURFACE-INDUCED ORDERING KINETICS

Now we turn to the question of how order evolves in a system with free surfaces. Quench conditions are chosen as in Section 3 with final temperatures below T_0 but in the vicinity of T_{sp} ($0.9 \lesssim T_f/T_0 \lesssim 1$). First, within few MC-steps B -atoms enrich in the surface layer to a concentration of about 50% and deplete in the adjacent layer, thereby establishing local equilibrium as enforced by the surface field h_1 . This implies $\psi_3 \simeq 1.85$ to about 1.9 at $z = 0$ in the temperature interval considered. This process in turn induces moves of B -atoms from even to odd layers within an increasing depth from the surface, thus forming a ψ_3 -front which penetrates into the bulk.

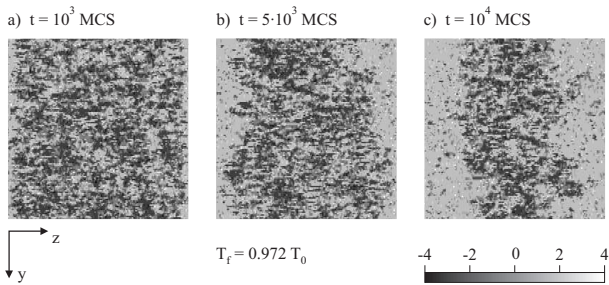


FIG. 4. ψ_3 -patterns at $T_f = 0.972 T_0$ for three different times after the quench, illustrating propagation of a surface-induced ordering wave.

As an example, we show in Fig. 4 the ψ_3 -distribution in a section parallel to the (y, z) -plane at $T_f = 0.972 T_0 > T_{sp}$ for three different times after the quench. The patterns clearly demonstrate a systematic progression of an

ordered state with fixed (positive) sign of ψ_3 . Taking averages over sheets parallel to the surface, we obtain profiles $\psi_3(z, t)$ which are plotted in Fig. 5. At $t = 10^4$ a plateau region for smaller z has evolved with ψ_3 -values in the vicinity of the equilibrium order parameter $\bar{\psi} \simeq 1.79$ at that temperature, before the profile decays to zero for larger z . Evidently, the thickness of the interface between the partially ordered state and the bulk (not penetrated by the ψ_3 -front) increases with time, an effect expected to arise both from growing intrinsic capillary wave fluctuations³³ and from bulk fluctuations in all three order parameter components with the character as in Fig. 2a, to be “incorporated” into the front during propagation.

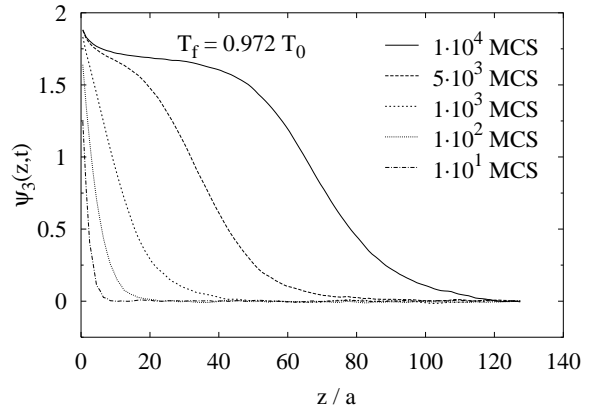


FIG. 5. Average profiles $\psi_3(z, t)$ for several times after the quench.

The profiles $\psi_3(z, t)$ allow us to define a time-dependent penetration depth $z_3(t)$ by setting $\psi_3(z_3(t), t) = \frac{1}{2}\psi_3(0, t)$. Plots of $z_3(t)$ for a series of final temperatures T_f are shown in Fig. 6a for a system large enough in the z -direction ($N = 64, M = 128$) to avoid the ψ_3 -fronts induced by both surfaces to overlap. (In fact, data in Fig. 5 and 6 contain an average over those two fronts.) As expected, after a quench not passing the phase boundary $z_3(t)$ rapidly saturates. For example, at $T_f = 1.006 T_0$ the final penetration depth is about 6 atomic layers, which is of the order of the bulk correlation length ξ in the disordered phase at that temperature. On the other hand, when $T_{sp} < T_f < T_0$, we see that after a short transient $z_3(t)$ grows more or less linearly with time within an extended time interval. This allows us to introduce a penetration velocity $v(T)$ which increases upon lowering the temperature. For example, at $T_f = 0.972 T_0$ we find that $z_3(t)$ grows linearly up to at least 10^4 MCS, where it reaches about 70 atomic layers, see also Fig. 4. In determining $v(T)$, shown in Fig. 7, care has to be taken with respect to the lateral size N of the system. For small N the system is likely to develop single (closed) domains in the lateral direction within the front region. Increased order of this type will

speed up the penetration process. This N -dependence of v is exemplified in Fig. 6b for $T_f = 0.972 T_0$. Data up to $t = 10^4$ MCS, however, seem to converge sufficiently at our largest $N = 128$. As seen from Fig. 7, when temperature is decreased from T_0 , the velocity $v(t)$ first increases with upward curvature, but decelerates when $T \approx T_{sp}$. Sufficiently below T_{sp} , linear growth can no longer be identified and $v(T)$ becomes undefined, see the case $T_f = 0.911 T_0$ in Fig. 6a. Some estimates based on mean-field arguments concerning the order of magnitude of $v(T)$ are presented in the Appendix.

When temperature falls near or below $T_f \simeq 0.963 T_0$, a new regime of slower growth beyond some crossover time t^* becomes detectable within the time window of Fig. 6. t^* decreases with temperature, so that the regime of linear growth shrinks. Notice in addition the non-monotonous behavior of $z_3(t)$ as a function of temperature for fixed observation time t . As indicated already, the strong shrinkage of the linear regime, where t^* tends to merge with the short time transient, occurs at temperatures slightly below but very near the spinodal temperature $T_{sp} \simeq 0.967$ discussed in Section 3 on the basis of static considerations. Regarding these surface phenomena we conclude that the spinodal temperature as estimated via the static segregation profiles separates two distinct dynamical regimes, roughly characterized by the presence or the absence of surface-induced linear (constant velocity) growth in an intermediate time domain.

The slowing down of the front motion beyond the linear regime, i.e. for $t > t^*$, clearly originates from its competition with nearly saturated domains that have already nucleated in the bulk. Crudely speaking, t^* will be determined by the interplay of two dynamic quantities, the penetration velocity $v(T)$ and the nucleation rate of ordered domains. Moreover, unstable growth of bulk domains at temperatures $T_f < T_{sp}$ totally suppresses the linear regime. To investigate this situation more closely, we carried out even longer runs up to $t = 2 \cdot 10^4$ for the case $T_f = 0.911 T_0$. Results at that temperature for $z_3(t)$ in a log-log representation are shown in Fig. 6c. The data in the range $t \gtrsim 2 \cdot 10^3$ MCS appear to follow a power-law $z_3(t) \simeq t^n$ with $n \simeq 0.27 \pm 0.02$. The appearance of such small growth exponent is confirmed by additional simulations at a temperature $T_f = 0.759 T_0$ considerably below T_{sp} , also shown in Fig. 6c. These data indicate in addition that the onset of this type of power law is moved to earlier times when temperature is lowered. Conversely, data for $T_f = 0.963 T_0$ display a crossover to a slow temporal growth compatible with $n \approx 1/4$ at a larger crossover time, indicated as t^* in Fig. 6c. Since the penetration depth up to $t = 2 \cdot 10^4$ stays significantly smaller than the system size (in this case $N = M = 128$), we expect that finite size effects do not play an essential role in estimating that exponent n . Preliminary results for the structure factor of a bulk system seem to confirm that value of n , although no definitive conclusions concerning the asymptotic long-time behavior can be drawn from these studies so far. Nevertheless

it is interesting to compare our findings in Fig. 6c with recent work by Castán and Lindgård.^{34,35}

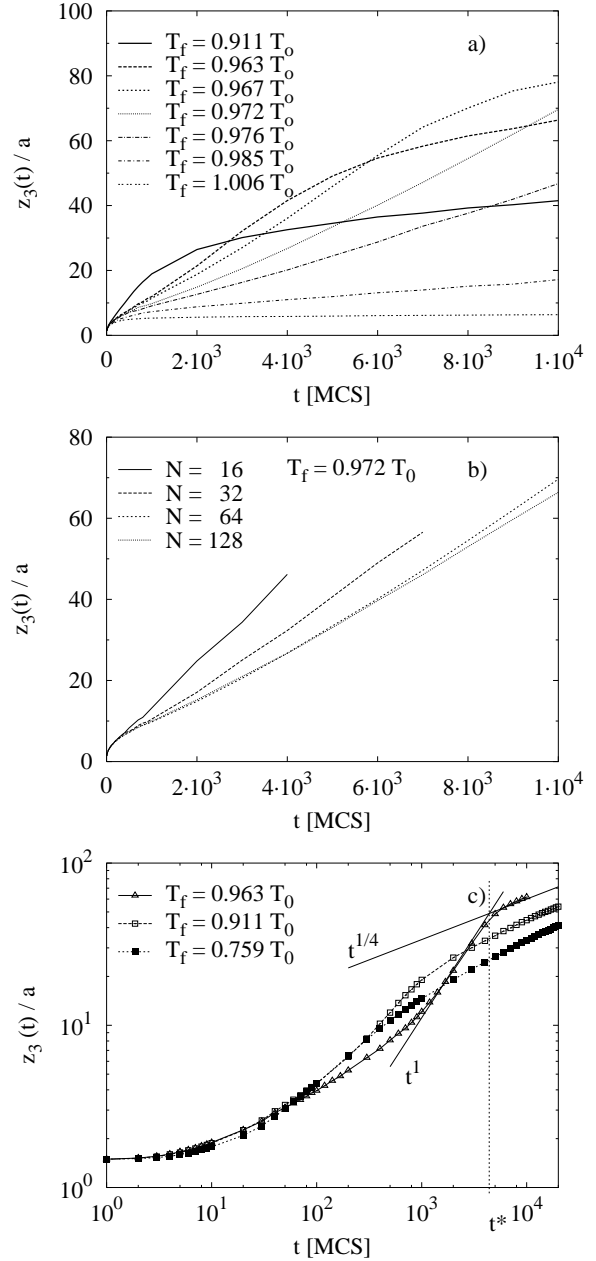


FIG. 6. (a) Time-dependent penetration depth $z_3(t)$ of the ψ_3 -front (see Fig. 5) for various final temperatures. (b) Dependence of $z_3(t)$ on the lateral system size N . (c) Time-dependent penetration depth in a double-logarithmic representation for three different temperatures. The growth behavior for large times (up to $t = 2 \cdot 10^4$ MCS for the two lower temperatures) is compared with a $t^{1/4}$ -law (straight line). At $T_f = 0.963 T_0$ a comparatively short time domain of linear growth appears (see the steeper straight line) up to the crossover time t^* .

These authors studied coarsening processes in a 2-dimensional system involving both curved and flat (zero

curvature) domain walls. The latter were essentially immobile and could be removed only by the progression of an intervening curved wall. Such a situation basically is encountered also in the present model, where type-1 antiphase boundaries turn out to be essentially immobile. This stability of flat walls induces an overall growth exponent which is smaller than the classical Lifschitz–Allen–Cahn exponent $n = 1/2$.^{36,37} Castán in fact gave arguments in favor of an exponent $n = 1/4$. A similar conclusion with respect to n was reached by Deymier et al.³⁸ from studies of a different model with two types of contacts between domains.

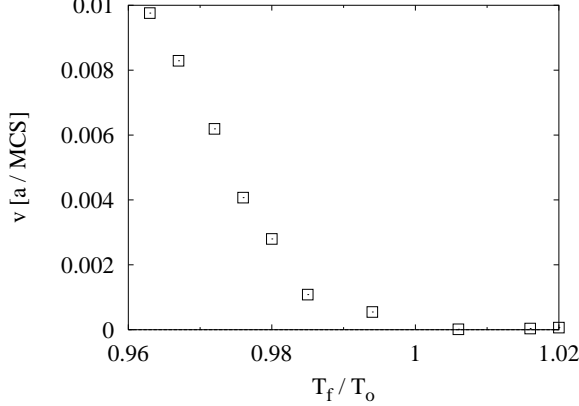


FIG. 7. Penetration velocity $v(T)$ versus temperature.

Next we study lateral ordering within layers parallel to the (xy) –plane at a depth z from the surface. This process proceeds in different ways depending on whether $z < z_3(t)$ or $z > z_3(t)$. When analyzing the layer $z = M$ midway between the two surfaces, representative for the latter case, we recover the characteristics of bulk ordering as described briefly in Section 3, see also Fig. 2. Our main objective, however, is the near-surface region $z < z_3(t)$ and consequences of the surface-induced segregation wave. As emphasized before,^{18,19} for $z < z_3(t)$ the sign of ψ_3 is essentially fixed to $\psi_3 > 0$ so that only two types of domains can appear: $(\psi_1, \psi_2, \psi_3)/\bar{\psi} = (1, -1, 1)$ and $(-1, 1, 1)$. These correspond to the two ways B –atoms can form a $(1, 1)$ –superstructure on the square lattice building an odd (AB –type) layer. Walls between those domains encountered when going in the lateral direction are exclusively of type 2, whereas type-1 walls are parallel to the surface. To analyze this situation further, we have enlarged the system in the lateral direction to $N = 256$, but restricted ourselves to $M = 8$ so that ψ_3 is nearly uniform along the z –axis. Patterns of all three order parameter components were extracted from atomic layers 7 and 8 midway between the two surfaces. An example with $T_f = 0.911 T_0$ and $t = 10^4$ MCS is shown in Fig. 8. In fact, domain walls in Figs. 8a and 8b with simultaneous sign changes of ψ_1 and ψ_2 are always curved, indicative of type-2 walls, and the domain structure appears completely isotropic, in contrast to the anisotropic shape of bulk domains (cf. Fig. 2). Fig. 8c depicts ψ_3 which is nearly constant.

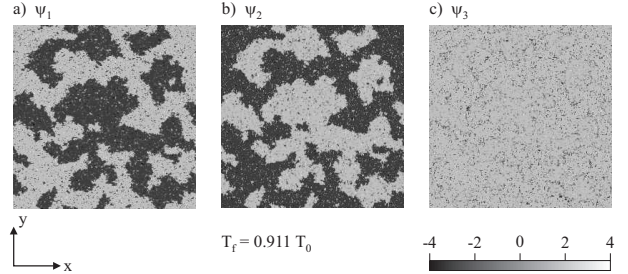


FIG. 8. Lateral domain patterns for a) ψ_1 and b) ψ_2 in the near-surface penetrated region with nearly uniform ψ_3 (see c)) at $T_f = 0.911 T_0, t = 10^4$ MCS. Notice the absence of type-1 walls (see text).

The time-dependent average size of domains in the (xy) –section of Fig. 8 is analyzed in Fig. 9, where we present results for the first moment

$$k_\alpha(z, t) = \frac{\sum_{k_\parallel} k_\parallel S_\alpha(k_\parallel, z, t)}{\sum_{k_\parallel} S_\alpha(k_\parallel, z, t)} \quad (6)$$

of the time-dependent lateral structure factor, defined by

$$S_\alpha(k_\parallel, z, t) = \langle |\psi_\alpha(k_\parallel, z, t)|^2 \rangle \quad (7)$$

where $\alpha = 1$ to 3 and $\psi_\alpha(k_\parallel, z, t)$ is the lateral Fourier transform of the local order parameter $\psi_\alpha(\vec{r}, t)$. Note that vacancy depletion in AB –type layers and enrichment in A –type layers (see Section 3) expands the overall time-scale for lateral ordering. While the behavior of $k_3(t)$ reflects a rapid transition to a near-uniform ψ_3 –distribution (see Fig. 8c), the data points for $k_\alpha(t)$ with $\alpha = 1, 2$ in Fig. 9 seem to approach a growth behavior $k_\alpha^{-1}(t) \sim t^n$ described by the Lifschitz–Allen–Cahn exponent $n = 1/2$. In fact, our results indicate curvature driven coarsening in the lateral directions, distinctly different from the perpendicular growth displayed in Fig. 6c.

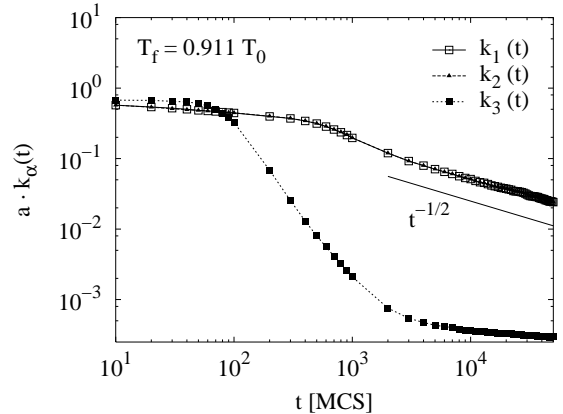


FIG. 9. First moments $k_\alpha(t)$ of lateral structure factors $S_\alpha(k_\parallel, z, t)$ in the same (x, y) –section as in Fig. 8, for $T_f = 0.911 T_0$. The behavior of $k_1(t) = k_2(t)$ at long times is compared with the Lifschitz–Allen–Cahn prediction (straight line).

5. SUMMARY AND CONCLUDING REMARKS

Surface-induced ordering processes in an fcc alloy model were studied on the basis of the atom–vacancy exchange mechanism. One essential result of our simulation studies is the appearance of a segregation wave induced at the surface and propagating into the bulk immediately after a temperature quench across the ordering temperature T_0 . This feature of our model qualitatively agrees with peculiar subsurface ordering phenomena at Cu₃Au (001) observed in recent X –ray experiments.¹⁸ In the region $z < z_3(t)$ covered by the segregation wave, the present model with nearest–neighbor interactions only shows an increased tendency to build up lateral order. The experimental verification of this effect may depend on the alloy material under consideration.

A second important conclusion confirmed by our simulations is the existence of an anisotropic domain structure in the near–surface region $z < z_3(t)$. Only two types of domains and, for z fixed, only high–energy domain walls appear, as opposed to the well–known domain structure in the bulk with 4 types of domains and both high– and low–energy walls in either direction. Since in Cu₃Au $z_3(t)$ can become larger than 200 Å¹⁸ or about 50 atomic layers (in our simulations more than 70 atomic layers) this should offer the possibility to grow films of mesoscopic thickness with an anisotropic domain structure not realized in the bulk. An interesting question for future work concerns films with odd and even numbers of atomic layers and overlapping ψ_3 –fronts induced by both surfaces.

Moreover, our present studies exemplify different ordering scenarios that may emerge more generally in systems whose bulk structure requires a multicomponent order parameter, and where the surface favors some kind of partial ordering. Concerning domain growth in our model, we have to distinguish between perpendicular and lateral growth modes, between a near–surface partially ordered region ($z < z_3(t)$) and the bulk region ($z > z_3(t)$), and between quench temperatures T_f above and below the spinodal temperature T_{sp} . At least three distinct coarsening schemes at intermediate or long times were observed. If $T_{sp} < T_f < T_0$, perpendicular order initially grows linearly with t such that $z_3(t) \simeq vt$ for $t < t^*$, while for $t > t^*$ our data indicate a temporal regime where $z_3(t) \sim t^{1/4}$. On the other hand, for $T_f < T_{sp}$ the regime of linear perpendicular growth is suppressed. Analysis of the typical domain structure in the lateral direction shows that in the region $z < z_3(t)$ it is isotropic and coarsens according to $k_\alpha^{-1}(t) \sim t^{1/2}$ at long times ($\alpha = 1; 2$) while for $z > z_3(t)$ one recovers bulk behavior.

Besides some open questions addressed already above we like to point out that non-stoichiometric alloys should in principle display even more rich and interesting behaviors, in particular in cases where ordering and phase separation occur simultaneously.³⁹

ACKNOWLEDGMENTS

The authors are indebted to H. Reichert for several discussions concerning the experimental situation and to P. Maass for helpful comments. A useful conversation with M. Maret, M. Albrecht and G. Schatz about surface segregation effects in the fcc alloy CoPt₃ is also gratefully acknowledged. This work was supported in part by the Deutsche Forschungsgemeinschaft, SFB 513.

APPENDIX

We attempt here to give some qualitative estimates concerning the magnitude of the penetration velocity $v(T)$, see Section 4, from simplified mean–field considerations. Our starting point are time–dependent Ginzburg–Landau equations, based on the free energy density $f(\psi_1, \psi_2, \psi_3)$ as given by Lai³¹ for the Cu₃Au structure,

$$f = \sum_{\alpha} \left(\frac{r}{2} \psi_{\alpha}^2 + \frac{v}{4} \psi_{\alpha}^4 \right) + \frac{u}{4} \left(\sum_{\alpha} \psi_{\alpha}^2 \right)^2 + w \psi_1 \psi_2 \psi_3 \quad (8)$$

with $r = r_0(T - T_{sp})$; $r_0 > 0$; $u > 0$; $|v| < u$; $w > 0$. The ordering temperature T_0 is determined by $r(T_0) = (2/9)w^2/(3u + v)$ and the order parameter at T_0 has the magnitude $|\psi_{\alpha}| = \bar{\psi}$ with $\bar{\psi} = (2/3)w(3u + v)$. Regarding the penetration of the segregation wave as a one–dimensional process along the z –axis (perpendicular to the surface), we assume an equation of motion for $\psi_3(z, t)$ of the form

$$\partial_t \psi_3 = -\Gamma \left(\frac{\partial f}{\partial \psi_3} - K \psi_3'' \right) \quad (9)$$

with a kinetic coefficient Γ and $K > 0$. Two limiting cases concerning the coupling of ψ_3 with ψ_1 and ψ_2 can be considered such that (9) becomes a closed equation for ψ_3 only. Thereby it turns out that the simulated velocity falls between these two limits. First, if the parameters are such that the evolution of lateral order, expressed by ψ_1 and ψ_2 , considerably lags behind the progression of the ψ_3 –front, one may set in (9) $\psi_1 = \psi_2 = 0$. In this case, the form (8) of the free energy density allows a nontrivial solution for a propagating front only at temperatures $T < T_{sp}$, with a velocity of propagation $v \propto (T_{sp} - T)^{1/2}$.¹⁹ Correspondingly, we obtain $v = 0$ for $T > T_{sp}$, contrary to Fig. 7. However, simulations of our nearest–neighbor interaction model indicate that lateral order at least on small length scales evolves almost simultaneously with the front motion in the perpendicular direction. This suggests to consider a second, in fact opposite limit, namely that ψ_1 and ψ_2 instantaneously relax towards the “local equilibrium condition” $\psi_1 = -\psi_2 = \pm \psi_3$. This yields the approximation $w\psi_1\psi_2 \simeq -w\psi_3^2$, to be used in (9). Introducing $\varphi = \psi_3/\bar{\psi}$ and the “potential”

$$\begin{aligned}
V(\varphi) &= -f/(3r(T_0)\bar{\psi}^2) = \\
&= \frac{1}{2}(1-r/r(T_0))\varphi^2 - \frac{1}{2}\varphi^2(\varphi-1)^2
\end{aligned} \tag{10}$$

we obtain

$$\partial_t \varphi = \Gamma r(T_0)(dV/d\varphi + (\xi(T_0))^2 \varphi'') \tag{11}$$

where $\xi_0 = (K/r(T_0))^{1/2}$ denotes the correlation length at T_0 . The ansatz $\varphi(z, t) = \eta(z - vt)$ leads to an ordinary differential equation for $\eta(z)$. The velocity v is determined in the usual manner⁴⁰ by requiring that appropriate boundary conditions can be fulfilled. These are $\eta(z) \rightarrow \eta_{\max}$; $\eta'(z) \rightarrow 0$ as $z \rightarrow -\infty$, where $\eta_{\max} > 0$ corresponds to the absolute maximum of $V(\eta)$ and $\eta(z) \rightarrow 0$; $\eta'(z) \rightarrow 0$ as $z \rightarrow \infty$. Numerical solution of this problem shows that, at T_0 , $v(T)$ starts to grow linearly in $T_0 - T$ and that $v(T_{sp}) \simeq 1.4\Gamma r(T_0)\xi_0$. To estimate Γ , one can formulate mean-field arguments for the diffusion of the slower atomic species, in this case the B -atoms, along the z -axis, which yields $D_B/a^2 \simeq 2\Gamma r(T_0)$. Using $\xi_0 \simeq 6a$, this gives the relation $v(T_{sp}) \simeq 4(D_B/a)$, independent of the Monte Carlo time unit. From the simulated value $D_B \simeq 0.04a^2/\text{MCS}$ at T_0 , see Fig. 3, we obtain $v(T_{sp}) \simeq 0.16a/\text{MCS}$. Comparison with Fig. 7 shows that these simple arguments overestimate the velocity at T_{sp} by about one order of magnitude. This is not surprising in view of the simplifications made, especially in view of the neglect of lateral fluctuations. These may strongly reduce the penetration velocity, an effect already inferred from the N -dependence of the velocity displayed in Fig. 6b.

¹ For a recent review see S. Puri and H. L. Frisch, *J. Phys.: Condens. Matter* **9**, 2109 (1997).
² H. P. Fischer, P. Maass and W. Dieterich, *Phys. Rev. Lett.* **79**, 893 (1997); *Europhys. Lett.* **42**, 49 (1998).
³ K. Binder, *Rep. Prog. Phys.* **50**, 783 (1987).
⁴ R. W. Cahn, *Nature* **342**, 619 (1989).
⁵ R. Lipowsky and D. A. Huse, *Phys. Rev. Lett.* **57**, 353 (1986).
⁶ R. Blossey, *Int. J. Mod. Phys. B* **9**, 3489 (1995).
⁷ W. Schweika, *Disordered Alloys: Diffuse Scattering and Monte Carlo Simulations*, Springer Tracts in Modern Physics **141** (Springer, Berlin Heidelberg, 1998).
⁸ H. Dosch, *Critical Phenomena at Surfaces and Interfaces*, Springer Tracts in Modern Physics **126** (Springer, Berlin Heidelberg, 1992).
⁹ H. Dosch, L. Mailänder, A. Lied, J. Peisl, F. Grey, R. L. Johnson, and S. Krummacher, *Phys. Rev. Lett.* **60**, 2382 (1988).
¹⁰ S. Dietrich, *Phase Transitions and Critical Phenomena*, **12**,

Eds. C. Domb and J. L. Lebowitz, Academic Press, London, 1988, pp 1-218.
¹¹ R. Lipowsky and W. Speth, *Phys. Rev. B* **28**, 3983 (1983).
¹² H. Reichert, P. J. Eng, H. Dosch and I. K. Robinson, *Phys. Rev. Lett.* **74**, 2006 (1995).
¹³ K. R. Mecke and S. Dietrich, *Phys. Rev. B* **52**, 2107 (1995).
¹⁴ M. Hayoun, V. Pontikis and C. Winter, *Surface Science* **398**, 125 (1998).
¹⁵ C. Seok and D. W. Oxtoby, *J. Phys.: Condens. Matter* **9**, 87 (1997).
¹⁶ M. Asta, G. Ceder and D. de Fontaine, *Phys. Rev. Lett.* **66**, 1798 (1991).
¹⁷ B. D. Gaulin, E. D. Hallman and E. C. Svensson, *Phys. Rev. Lett.* **64**, 289 (1990).
¹⁸ H. Reichert, P. J. Eng, H. Dosch and I. K. Robinson, *Phys. Rev. Lett.* **78**, 3475 (1997).
¹⁹ H. P. Fischer, J. Reinhard, W. Dieterich and A. Majhofer, *Europhys. Lett.* **46**, 755 (1999).
²⁰ K. Yaldram and K. Binder, *Z. Phys. B* **82**, 405 (1991).
²¹ K. Yaldram and K. Binder, *J. Stat. Phys.* **62**, 161 (1991).
²² P. Fratzl and O. Penrose, *Phys. Rev. B* **50**, 3477 (1994); *Phys. Rev. B* **55**, R6101 (1997).
²³ M. Plapp and J.-F. Gouyet, *Phys. Rev. Lett.* **78**, 4970 (1997).
²⁴ S. Puri and R. Sharma, *Phys. Rev. E* **57**, 1873 (1998).
²⁵ C. Frontera, E. Vives, T. Castán, and A. Planes, *Phys. Rev. B* **55**, 212 (1997).
²⁶ S. Engemann, H. Reichert, H. Dosch, H. Hong, Z. Wu and H. Chen, to be published.
²⁷ The Hamiltonian (1) is equivalent with the Blume-Emery-Griffiths model, see M. Blume, V. J. Emery and R. B. Griffith, *Phys. Rev. A* **4**, 1071 (1971).
²⁸ W. Schweika and D. P. Landau in *Computer Simulation Studies in Condensed Matter Physics X*, edited by D. P. Landau, K. K. Mon and H.-B. Schüttler (Springer, Berlin Heidelberg, 1998) p 186-190.
²⁹ K. Binder, *Phys. Rev. Lett.* **45**, 811 (1980).
³⁰ In a good approximation the main decay of the segregation profile towards the bulk follows an exponential, $\psi_3 \propto \exp(-z/\xi(T))$, as long as $T > T_{cs}$. In the case $T < T_{cs}$, $\xi(T)$ was extracted from the tails of the ψ_3 -profiles.
³¹ Z.-W. Lai, *Phys. Rev. B* **41**, 9239 (1990).
³² Th. Heumann and Th. Rottwinkel, *J. Nucl. Matter* **69-70**, 567 (1978).
³³ J. S. Rowlinson, and B. Widom, in *Molecular Theory of Capillarity* (Calderon, Oxford, 1982).
³⁴ T. Castán and P.-A. Lindgård, *Phys. Rev. B* **40**, 5069 (1989).
³⁵ T. Castán and P.-A. Lindgård, *Phys. Rev. B* **43**, 956 (1991).
³⁶ I. M. Lifshitz, *Sov. Phys. JETP* **15**, 939 (1962).
³⁷ S. M. Allen and J. W. Cahn, *Acta Metall.* **27**, 1085 (1979).
³⁸ P. A. Deymier, J. O. Vasseur, and L. Dobrzynski, *Phys. Rev. B* **55**, 205 (1997).
³⁹ H. P. Fischer and W. Dieterich, *Phys. Rev. E* **56**, 6909 (1997).
⁴⁰ G. Dee and J. S. Langer, *Phys. Rev. Lett.* **50**, 383 (1983).